ISSN 1063-7761, Journal of Experimental and Theoretical Physics, 2010, Vol. 111, No. 4, pp. 635–644. © Pleiades Publishing, Inc., 2010.
Original Russian Text © S.V. Nikolaev, S.G. Ovchinnikov, 2010, published in Zhurnal Éksperimental'noĭ i Teoreticheskoĭ Fiziki, 2010, Vol. 138, No. 4, pp. 717–728.

ELECTRONIC PROPERTIES OF SOLID

Cluster Perturbation Theory in Hubbard Model Exactly Taking into Account the Short-Range Magnetic Order in 2 × 2 Cluster

S. V. Nikolaev[a,b,*] and S. G. Ovchinnikov[a,c]

[a] *Kirenskii Institute of Physics, Siberian Branch, Russian Academy of Sciences, Krasnoyarsk, 660036 Russia*
[b] *Dostoevsky State University, Omsk, 644077 Russia*
[c] *Siberian Federal University, Krasnoyarsk, 660041 Russia*
**e-mail: 25sergeyn@mail.ru*

Received December 17, 2009

Abstract—The cluster perturbation theory is presented in the 2D Hubbard model constructed using X operators in the Hubbard-I approximation. The short-range magnetic order is taken into account by dividing the entire lattice into individual 2 × 2 clusters and solving the eigenvalue problem in an individual cluster using exact diagonalization taking into account all excited levels. The case of half-filling taking into account jumps between nearest neighbors is considered. As a result of numerical solution, a shadow zone is discovered in the quasiparticle spectrum. It is also found that a gap in the density of states in the quasiparticle spectrum at zero temperature exists for indefinitely small values of Coulomb repulsion parameter U and increases with this parameter. It is found that the presence of this gap in the spectrum is due to the formation of a short-range antiferromagnetic order. An analysis of the temperature evolution of the density of states shows that the metal–insulator transition occurs continuously. The existence of two characteristic energy scales at finite temperatures is demonstrated, the larger scale is associated with the formation of a pseudogap in the vicinity of the Fermi level, and the smaller scale is associated with the metal–insulator transition temperature. A peak in the density of states at the Fermi level, which is predicted in the dynamic mean field theory in the vicinity of the metal–insulator transition, is not observed.

DOI: 10.1134/S1063776110100146

1. INTRODUCTION

It has become clear in recent decades that correlation effects play a leading role in the formation of physical properties of a large group of materials with strong electron correlations (in particular, high-temperature superconductors). The quasi-two-dimensional structure of HTSC cuprates is also an important factor determining the properties of these materials.

The most promising model for theoretical study of quasi-two-dimensional systems with strong electron correlations is the two-dimensional (2D) Hubbard model [1]. In spite of its apparent simplicity, this model helps to reveal general fundamental properties of these materials. An important constraint in a detailed theoretical description of properties of strongly correlated systems is the fact that the kinetic and potential energies are of the same order of magnitude. This means that perturbation theory is applicable neither in the weak coupling limit nor in the strong coupling limit. However, it is well known that an analysis of 2D systems based on the theories of dynamic mean field, which are most advanced theories in the Hubbard model [2–4], is impossible due to the disregard of spatial correlations of particles in this theory. A large number of recent publications devoted to the development of a new class of theories can be classified as quantum cluster theories [5]. The very idea of dividing the entire lattice into clusters and to take into account the interaction in a cluster and the interaction between clusters in perturbation theory was presented long ago [6–8]. Later, a number of theories were developed based on this principle, e.g., the cluster dynamic mean field theory (CDMFT) [9], dynamic cluster approximation (DCA) [10], and cluster perturbation theory (CPT) [11]. An analogous approach was used in [12] for describing plaquette deformation of a 2D quantum magnet.

In these theories, the first step is the division of the entire lattice into cluster and taking into account intracluster interactions exactly. For this purpose, the Lanczos method [13, 14] of exact diagonalization was mainly used. It is shown below that this approach is not correct without an appropriate control of the number of states in the Hilbert state and may lead to incorrect results. For this reason, the exact complete diagonalization method taking into account all excited states in each subspace of the Hilbert state of local cluster states is used in our study.

The second step in constructing cluster theories is the allowance for interactions between clusters. At this stage, all quantum cluster theories differ significantly. For example, in CDMFT and DCA, a self-consistent approach is used to take into account the interaction

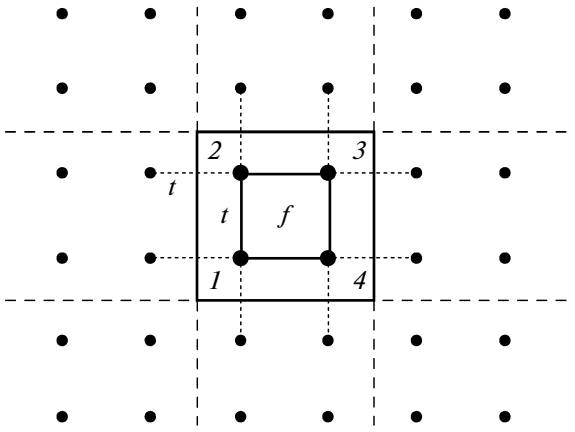

Fig. 1. Division of lattice into 2×2 clusters. Interaction between nearest neighbors in a cluster is shown by solid lines and interaction between clusters is shown by dashed lines.

of a cluster with the surroundings, while in the CPT, this interaction is taken into account without the self-consistent procedure in perturbation theory using the concept of auxiliary fermions [15]. We will use the technique of Hubbard X operators, which makes it possible to write the interaction between clusters directly and precisely in the language of X operators. Further analysis of the model in the cluster representation can be carried out using various approximate procedures developed for the Hubbard model.

It should be noted that we operate in the framework of the 2D Hubbard model in the Hubbard-I approximation for intercluster jumps and confine our analysis to the case of half-filling (without doping). However, even in this simple (at first glance) version, the cluster approach has made it possible to slightly clarify this important physical phenomenon as the metal–insulator (Mott—Hubbard) transition and revealed interesting features of the electron band structure. In particular, we will demonstrate the existence of two characteristic energy scales at finite temperatures; the larger scale is associated with the formation of a pseudogap in the vicinity of the Fermi level, while the smaller scale is associated with temperature of the metal–insulator transition.

In Section 2, the exact diagonalization method is described. In Section 3, Hubbard X operators are constructed and a transition to this representation in the 2D Hubbard model is made. In Section 4, a Fourier transition to the lattice representation and from the reduced to extended Brillouin zone is described. In Section 5, the results of numerical calculation of the band structure of a 2D lattice are described, and the dependence of the gap width on the Coulomb interaction parameter U at a site is considered. The analogy between the spin density wave with a long-range magnetic order and the given situation with a short-range order is traced. Spin correlation functions for a cluster are calculated. In Section 6, the temperature dependences of the density of states are considered and it is shown that the metal–insulator transition occurs continuously. The temperature of this transition is determined and its dependence on parameter U is constructed. The results are discussed in the conclusion.

2. EXACT DIAGONALIZATION

Let us consider the 2D Hubbard model

$$H = H_0 + H_1, \tag{1}$$

$$H_0 = \sum_{i\sigma}\left\{(\varepsilon - \mu)n_{i\sigma} + \frac{U}{2}n_{i\sigma}n_{i\bar{\sigma}}\right\}, \tag{2}$$

$$H_1 = \sum_{i \neq j,\, \sigma} t_{ij} a^{\dagger}_{i\sigma} a_{j\sigma}, \tag{3}$$

where $a^{\dagger}_{i\sigma}$ and $a_{i\sigma}$ are the production and annihilation operators for an electron with spin σ at site i, $n_{i\sigma}$ is the density operator of electrons with spin σ ($\bar{\sigma} = -\sigma$), ε is the energy of an electron at a site, μ is the chemical potential, t_{ij} is the hopping integral, and U is the parameter of the Coulomb interaction at a site. In further analysis, we will confine ourselves to only the nearest neighbor approximation with jump amplitude t.

Let us pass from the single-site description to the cluster description. We divide the square lattice into 2×2 clusters (Fig. 1). It should be noted in this connection that the choice of this type of clusters preserves the point symmetry group of the initial lattice. Let us regroup the terms in Hamiltonian (1) to separate the intracluster interactions from intercluster interactions,

$$H = \sum_{f} H^{c}_{0}(f) + \sum_{f \neq g} H^{c}_{t}(f, g), \tag{4}$$

where f and g are the cluster indices. In further analysis, we will normalize energy to hopping parameter t, assuming that the latter is -1.

The next step after the division of the lattice into clusters is the exact solution of the time-independent Schrödinger equation with the intercluster part of Hamiltonian (4). After an exact diagonalization procedure, we obtain exact cluster wave eigenfunctions and corresponding energy eigenvalues. In connection with this, it should be emphasized that, in exact diagonalization, we do not use the Lanczos method, in which only the ground state and several excited states are determined precisely. Therefore, in our case, eigenvectors form an exact complete set.

For $N = 4$, the cluster wavefunction can be written as the sum of three terms containing homeopolar (with one electron per site), heteropolar (with a pair of electrons), and doubly heteropolar parts (with two pairs of electrons per site). In the limit $U \longrightarrow \infty$, only

homeopolar states are left, and wavefunction $|4^0\rangle$ has the form [12]

$$|4^0\rangle = \frac{1}{2\sqrt{3}}\{|\downarrow\downarrow\uparrow\uparrow\rangle - 2|\downarrow\uparrow\downarrow\uparrow\rangle + |\downarrow\uparrow\uparrow\downarrow\rangle + |\uparrow\downarrow\downarrow\uparrow\rangle - 2|\uparrow\downarrow\uparrow\downarrow\rangle + |\uparrow\uparrow\downarrow\downarrow\rangle\}. \quad (5)$$

Corrections to homeopolar function (5) were obtained analytically for $t \ll U$ in [6, 7].

3. CONSTRUCTION OF X OPERATORS

Since cluster wavefunctions form a complete orthonormal basis, by definition, we can construct Hubbard X operators for a cluster in the form

$$X_f^\alpha \equiv X_f^{pq} = |p\rangle\langle q|, \quad (6)$$

where f is the cluster index; $\alpha = \alpha(p, q)$, and p and q are the initial and final state, respectively. The properties of X operators be described in greater detail in [1, 16–18].

Let us write the Fermi annihilation operator in terms of the X operators,

$$a_{f\sigma i} = \sum_\alpha \gamma_{i\sigma}(\alpha) X_f^\alpha, \quad (7)$$

$$\gamma_{i\sigma}(\alpha) = \langle m', N-1|a_{i\sigma}|m, N\rangle, \quad (8)$$

where i is the intracluster index assuming values 1, 2, 3, and 4, and σ is the spin index. Here, it is shown explicitly that matrix element $\gamma_{i\sigma}(\alpha)$ determines transitions from a part of the Hilbert space with N particles in state m to the part of the Hilbert space with $N-1$ particles in state m'. The production operator can be written analogously.

Using the anticommutation relation between the Fermi production and annihilation operators, we can write the following sum rule:

$$\langle [a_{f\sigma i}, a_{f\sigma i}^\dagger]_+\rangle = 1 = \sum_\alpha |\gamma_{i\sigma}(\alpha)|^2 F(\alpha) \equiv f, \quad (9)$$

$$F(\alpha) = \langle X^{pp}\rangle + \langle X^{qq}\rangle, \quad (10)$$

where $F(\alpha)$ is the filling factor [17, 18]. Here, we have introduced the f factor, i.e., the quantity that determines the extent to which the sum rule (expressing the conservation of the total spectral weight of the electron) is observed. Calculations show that to obtain a correct result, we must control this quantity from 0.99 to 1.00 (see Section 5 for details). It follows from relation (9) that the f factor is accumulated due to an increase in the number of transitions from one part of the Hilbert space to another (Fig. 2). Consequently, the situation becomes possible, in which the f factor is already close to 1.0, but not all transitions are taken into account. This means that the remaining transitions are unlikely and do not make a considerable contribution to the total band pattern. This conclusion is confirmed by the results of calculations obtained in this study.

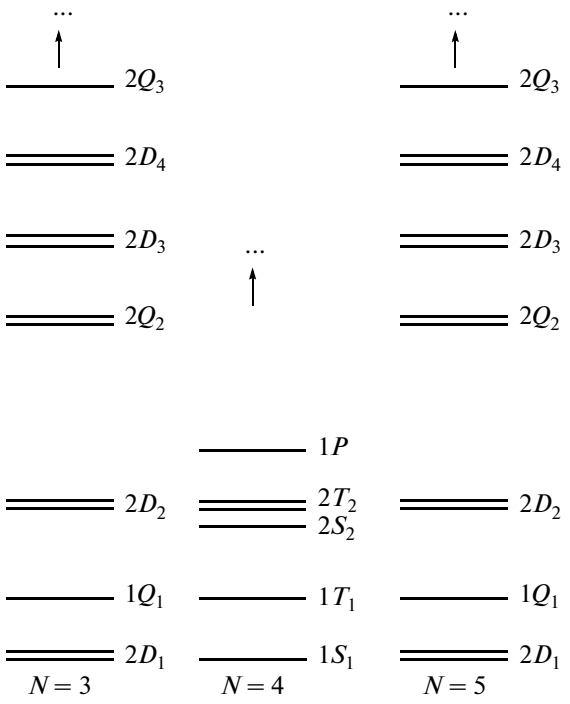

Fig. 2. Low-energy part of the Hilbert space with $N = 3$, 4, and 5 for $U = 8$ (notation: S, total spin is 0; D, 1/2; T, 1; Q, 3/2; and P, 2; the number on the left indicates degeneracy at the point symmetry group of the cluster).

Figure 2 shows the low-energy part of the Hilbert space for $N = 3$, 4, and 5 in the energy range of about $U/2$ relative to the lower energy level for each subspace. Here, the following scheme is used for denoting a state: the number on the left indicates degeneracy associated with the point symmetry group of the cluster, the letter indicates the total spin and the corresponding spin degeneracy multiplicity, and the subscript indicates the number of states with identical total spins. In the subspace with $N = 4$, the ground state is singlet S_1 (in the notation used in [6, 7], it is the term $|4^0\rangle$).

4. TRANSITION TO LATTICE

Having defined the X operators on a cluster, we can now write Hamiltonian (4) in the form

$$H = \sum_{fn} \varepsilon_n X_f^{nn} + \sum_{f\neq g}\sum_{\alpha\beta} t_{fg}^{\alpha\beta} X_f^\alpha X_g^{-\beta}, \quad (11)$$

where ε_n is the energy of a cluster in state n, and $t_{fg}^{\alpha\beta}$ are intercluster hopping integrals.

Let us carry out the Fourier transformation of X operators. We take into account the fact that these operators are defined for the clusters forming a qua-

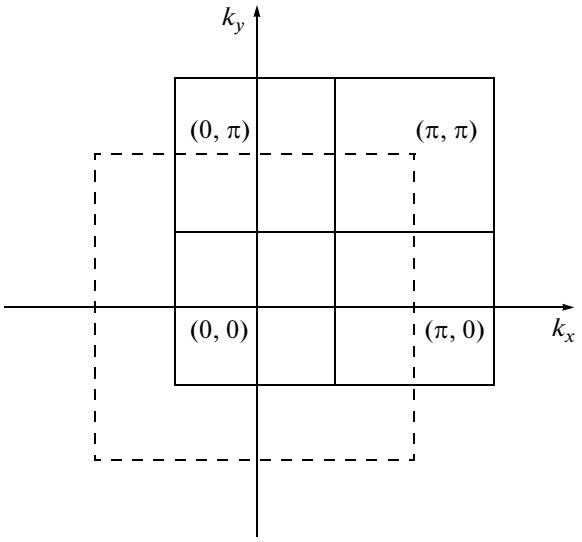

Fig. 3. Initial Brillouin zone (dashed lines), reduced Brillouin zone (solid lines) for the cluster superlattice.

dratic superlattice with a period twice as large as that of the initial lattice of sites. In our case, the number of sites in a cluster is four; consequently, the total number of clusters is smaller than the initial number of sites also by a factor of four. Taking into account this circumstance, we obtain

$$X_f^\alpha = \frac{1}{\sqrt{N^*}}\sum_{\tilde{\mathbf{k}}} e^{i\tilde{\mathbf{k}}\cdot\mathbf{R}_f} X_{\tilde{\mathbf{k}}}^\alpha, \tag{12}$$

where N^* is the number of clusters in the superlattice and $\tilde{\mathbf{k}}$ is the wave vector assuming the values in the reduced Brillouin zone (Fig. 3). As a result, we obtain

$$H = \sum_{\tilde{\mathbf{k}}}\sum_n \varepsilon_n(\tilde{\mathbf{k}}) X_{\tilde{\mathbf{k}}}^{nn} + \sum_{\tilde{\mathbf{k}}}\sum_{\alpha\beta} T_{\alpha\beta}(\tilde{\mathbf{k}}) X_{\tilde{\mathbf{k}}}^\alpha X_{\tilde{\mathbf{k}}}^{-\beta}. \tag{13}$$

Let us define two two-time Green's functions on the Fermi production and annihilation operators and for Hubbard fermions in the representation of X operators:

$$G(if, t; jg, t') = \langle\langle a_{if}(t) | a_{jg}^\dagger(t')\rangle\rangle, \tag{14}$$

$$D^{\alpha\beta}(f, t; g, t') = \langle\langle X_f^\alpha(t) | X_g^{-\beta}(t')\rangle\rangle, \tag{15}$$

where i and j are the intracluster indices and f and g are the cluster indices. Here, we have used the notation from [19].

After writing the equations of motion for Green function (15) and using the Fourier transform (12), we can obtain the following matrix equation in the Hubbard-I approximation:

$$D^{-1}(\tilde{\mathbf{k}}, \omega) = (D^0(\omega))^{-1} - T(\tilde{\mathbf{k}}), \tag{16}$$

where

$$D_{\alpha\beta}^0(\omega) = \frac{F(\alpha)}{\omega - \Omega(\alpha)}\delta_{\alpha,\beta}, \tag{17}$$

$$\Omega(\alpha) = \varepsilon_q(N+1) - \varepsilon_p(N) - \mu, \tag{18}$$

$$F(\alpha) \equiv F(p, q) = \langle X^{pp}\rangle + \langle X^{qq}\rangle. \tag{19}$$

Expression (17) defines the cluster Green function, which can be evaluated precisely and contains the energy of the transition (quasiparticle energy) from state q with number of particles $N + 1$ to state p with number of particles N (18), as well as filling factor (19) for Fermi quasiparticles, which is defined as the sum of filling factors of the corresponding states. This Green's function has the form of a diagonal matrix.

Let us define the Fourier transform for the Fermi operators

$$a_{f\sigma i} = \frac{1}{\sqrt{N_0}}\sum_{\mathbf{k}} a_{\mathbf{k}\sigma} e^{i\mathbf{k}\cdot(\mathbf{R}_f + \mathbf{r}_i)}, \tag{20}$$

where N_0 is the number of sites in the initial lattice and $\mathbf{k}$ is the wavevector defined in the initial Brillouin zone (see Fig. 3). It should be noted that this Fourier expansion for X operators (12) is defined in the reduced Brillouin zone. Green's function (15) is found to be defined for the superlattice of clusters. To pass to electron Green's function (14), we must establish the relation between Green's functions (14) and (15). Using expansion (7), we can obtain

$$G_{\sigma\sigma'}(if, t; jg, t') = \sum_{\alpha\beta}\gamma_{\sigma i}(\alpha)\gamma_{\sigma' j}(\beta) D^{\alpha\beta}(f, t; g, t'). \tag{21}$$

After Fourier transformation (20) taking into account expression (21), we can write the Fourier transform of the electron Green function as

$$G_\sigma(\mathbf{k}, \omega) = \frac{1}{N_c} \times \sum_{\alpha\beta}\sum_{ij}\gamma_{\sigma i}(\alpha)\gamma_{\sigma j}(\beta) e^{-i\mathbf{k}\cdot(\mathbf{r}_i - \mathbf{r}_j)} D_{\alpha\beta}(\mathbf{k}, \omega), \tag{22}$$

where N_c is the number of sites in the cluster (which is four in our case).

Having determined the electron Green function from formula (22), we can obtain the spectral function

$$A(\mathbf{k}, \omega) = -\frac{1}{\pi}\lim_{\eta\to 0^+}(\mathrm{Im}G(\mathbf{k}, \omega + i\eta + \mu)). \tag{23}$$

It is well known that the spectral function must obey the sum rule obtained from the anticommutation relation for the Fermi operators as follows:

$$\int d\omega A(\mathbf{k}, \omega) = \langle [a_{\mathbf{k}\sigma}, a_{\mathbf{k}\sigma}^\dagger]_+\rangle = 1. \tag{24}$$

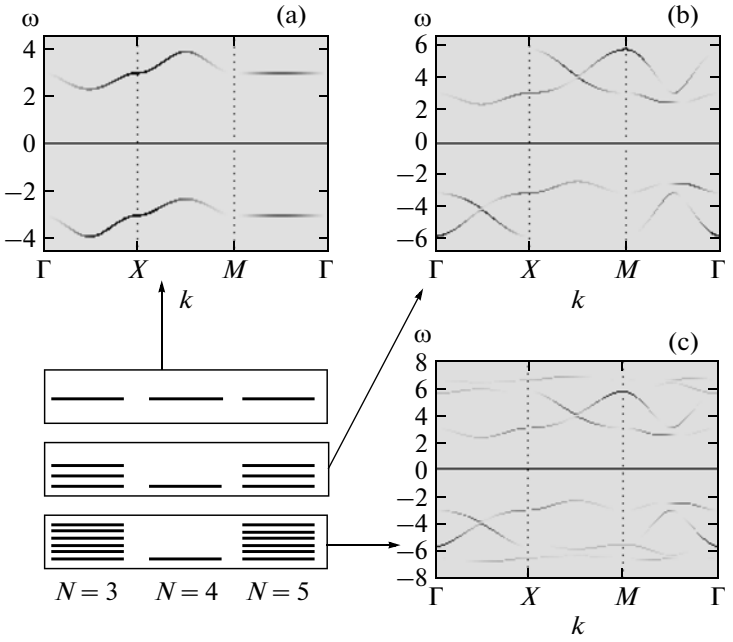

Fig. 4. Dependence of dispersion relation on number of accountable transitions (*f* factor): $f = 0.395$ (a), 0.792 (b), 0.9995 (c); $U = 8$. States in Hilbert space, the transitions between which were taken into account in calculating the relevant dispersion relations, are shown schematically.

Above, we have introduced the concept of *f* factor (9), which defines the extent to which equality (24) is satisfied, i.e.,

$$\int d\omega A(\mathbf{k}, \omega) = f. \quad (25)$$

We can now fully estimate the necessity of monitoring the *f* factor at the first steps of computation of the complete Green function. After the exact diagonalization of a cluster and before calculating the Green function, we can choose this number of Fermi quasiparticles (Hubbard fermions described by transitions $N + 1 \longrightarrow N$ in the Hilbert space; see Fig. 2), which will allow us to obey the sum rule at the end of calculations. In an ideal situation, we must include all transitions of the Hilbert space in our analysis. However, since we perform numerical calculations in which an increase in the number of transitions involves an increase the computation time, it is very important to determine the optimal number of transitions before calculations without noticeably affecting the final result. This is ensured by controlling the *f* factor at the beginning of numerical calculations. Examples of this control are given in the next section.

5. DISPERSION RELATIONS

One of the main methods for determining the physical properties of any substance is the construction and analysis of the dispersion relations for quasiparticles. In accordance with definition (17), the dispersion equation has the form

$$\det((\omega - \Omega(\alpha))\delta_{\alpha\beta} - F(\alpha)T_{\alpha\beta}(\tilde{\mathbf{k}})) = 0. \quad (26)$$

The solution to this equation gives bare dispersion relations for all quasiparticles. This set contains both dispersion relations hat define the bands, as well as dispersion-free levels. In other words, Eq. (26) also gives false poles, which are cancelled out with the numerator in the complete Green function. Spectral function (23) makes it possible to find the spectral weight of all such states for each value of the wavevector and, hence, to select physically significant poles.

Let us consider once again the influence of the *f* factor on the final result of calculation and the applicability of the Lanczos exact diagonalization method. It should be recalled that the magnitude of the *f* factor is affected by the number of accountable transitions between states differing by one particle in the Hilbert space. In the case of half-filling for a 2×2 cluster, these are transitions from states with $N = 5$ to the state with $N = 4$ and from states with $N = 4$ to those with $N = 3$ (see Fig. 2). At zero temperature, the filling factor of state $1S_1$ in the subspace with $N = 4$ is unity, while all remaining states are unfilled. The allowance for quantum fluctuations leading to a number of pairs on the order of $(t/U)^2$ in the limit of strong correlations is beyond the accuracy of our approximation.

Figure 4 shows the dependence of the dispersion relation on the number of accountable transitions. Here, the following notation for the characteristic points of the Brillouin zone is used: $\Gamma \equiv (0, 0)$, $X \equiv (\pi, 0)$, and $M \equiv (\pi, \pi)$. It can be seen that a gradual increase in the number of transitions (i.e., an increase in the *f* factor) leads to considerable changes in the band structure, including changes in dispersion relations

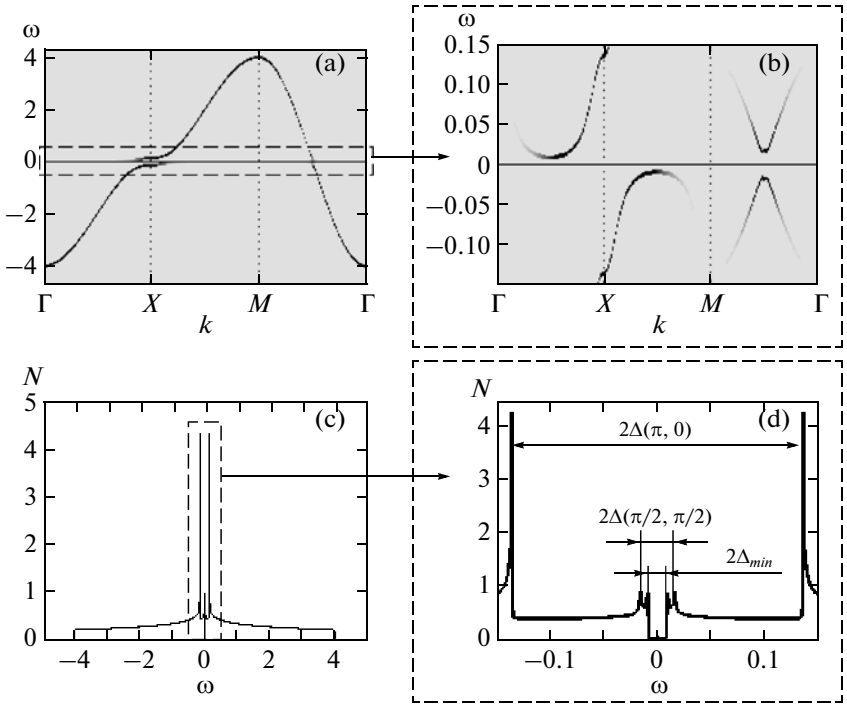

Fig. 5. (a) Dispersion curves ($U = 0.5, f = 0.997$); (b) enlarged dispersion region near the Fermi level; (c) density of states ($U = 0.5, f = 0.997, \delta = 0.0001$); (d) enlarged region of density of states for $U = 0.5$.

and the redistribution of weight among them; however, the result is qualitatively correct for all dispersion relations presented in the figure. This is primarily manifested in the formation of the upper and lower Hubbard bands. Thus, the uncontrollable rejection of excited states may lead to violation of the sum rule and a variation of the band pattern in the whole. This is precisely what occurs when we use the Lanczos exact diagonalization method, in which only the ground state and several excited states can be determined precisely due to the limitations of the method itself.

Figure 4c shows the band structure for six transitions to the half-space with a number of particles smaller by one, which forms the lower Hubbard band, and six transitions to the subspace with a number of particles larger by one, which forms the upper Hubbard band. In this case, the f factor is 0.9995, which indicates that a larger number of accountable transitions hardly changes the band structure. In fact, our calculations, which take into account all remaining transitions, shows that the emerging new states are dispersion-free, have almost zero spectral weight, and do not change the band structure.

An analysis of the dispersion relations and the density of states revealed a number of interesting features. Figure 5 shows the dispersion curves taking into account the spectral weight and the corresponding density of states for Coulomb repulsion parameter $U = 0.5$. As usual, in numerical calculations of the spectral function and the density of states, the delta function is replaced by the Lorentzian with half-width δ. In Fig. 5, this parameter is 0.0001. Let us consider Fig. 5a in greater detail, which clearly shows the band of free electrons for the limiting case $U = 0$ with a peak at point (π, π), a minimum at point (0, 0), and saddle point $(\pi, 0)$. At the same time, a weak shadow band can also be seen (Fig. 5b), which takes a part of the spectral weight from the main dispersion. The formation of the shadow band is associated with the presence of the antiferromagnetic order. However, in the 2D considered here, a long-range order can appear only at zero temperature in accordance with the Mermin–Wagner theorem. We calculate the electron structure under the assumption of the absence of a long-range magnetic order. Consequently, the shadow band can only appear due to the formation of the short-range antiferromagnetic order.

Figure 5c clearly shows two symmetric singularity, which merge together in the limit $U = 0$, forming a logarithmic divergence of the density of states at the Fermi level, which is typical in this limit. Figure 5d shows an enlarged region of the density of states near the Fermi level. The fine structure with several singularities can be seen clearly. We can single out three characteristic scales of the gap, i.e., a gap at point $(\pi, 0)$ between the saddle singularities on dispersion curves (see Fig. 5b), a gap in the vicinity of point $(\pi/2, \pi/2)$, and a minimal gap responsible for the actual gap in the density of states. It can be seen from Fig. 5b that the latter gap is not optical and is determined by the segments of dispersion curves with a small spectral weight at points $(\pi/2, 0)$ and $(\pi, \pi/2)$.

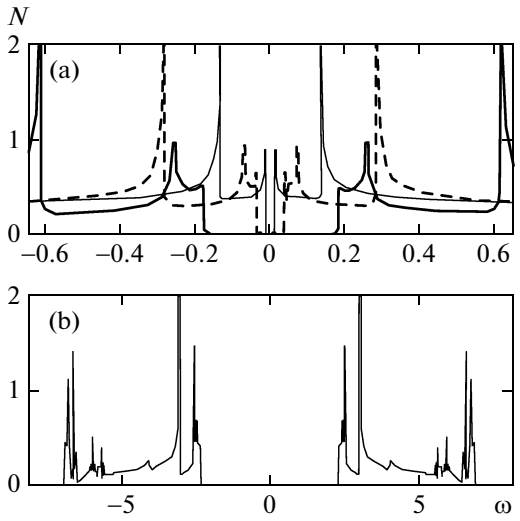

Fig. 6. Dependence of density of states on parameter U at $T = 0$: (a) fine curve ($U = 0.5$), dashed curve ($U = 1$), and bold curve ($U = 2$); $f > 0.995$; (b) $U = 8$, $f = 0.9995$.

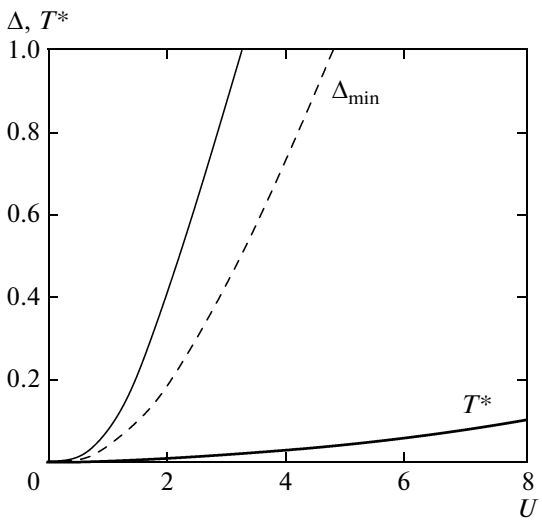

Fig. 7. Dependence of gap width (solid curve corresponds to the SDW state (27); dashed curve represents our numerical result for Δ_{min} due to short-range antiferromagnetic order) and metal–insulator transition temperature T^* (bold solid curve) on parameter U.

A detailed analysis of the dependence of minimal gap width Δ_{min} on parameter U shows that the gap in the density of states at zero temperature exists for indefinitely small values of U and increases with this parameter (Fig. 6). This behavior can be compared with the behavior of the gap which opens in the spectrum of states in the mean field theory due to the formation of a spin density wave (SDW). At zero temperature, we can find the SDW gap from the equation

$$\frac{1}{U} = \frac{1}{N}\sum_k \frac{1}{\sqrt{\varepsilon_0^2(\mathbf{k}) + \Delta^2}}, \tag{27}$$

$$\varepsilon_0(\mathbf{k}) = 2t(\cos k_x a + \cos k_y a). \tag{28}$$

We can obtain the dependence of this gap on parameter U (Fig. 7). In formulas (27) and (28), wavevector $\mathbf{k}$ runs over the antiferromagnetic Brillouin zone. It can be seen that the behavior of both gaps with increasing U is qualitatively the same, but our theoretical curve lies below the curve calculated by formula (27). For small values of parameter U, the dependence is exponential, while for large values of U, it becomes linear. Figure 7 also shows the temperature of transition from insulator to metal upon an increase in U (see below).

The calculation of the spin correlation functions of nearest neighbors in a cluster revealed the formation of a short-range antiferromagnetic order. The verification of the relation $\langle S_0^+ S_n^- \rangle = 2\langle S_0^z S_n^z \rangle$ shows that this system exhibits the properties of an isotropic spin liquid, for which the mean value of any spin component is zero, and the correlation functions are the same for the x, y, and z projections of spin.

6. TEMERATURE EVOLUTION OF THE DENSITY OF STATES

In the previous section, we have already considered the fine structure of the density of states and obtained the dependence of the gap width on Coulomb repulsion parameter U. We will now consider the temperature variations in the density of states, which lead to one more very important physical phenomenon, viz., metal–insulator transition.

Above all, we must explain how the temperature can affect the system. In all approximate approaches, some contributions to the self-energy part (that ensures, among other things, damping of quasiparticles upon an increase in temperature) are discarded. For this reason, in most publications devoted to analysis of the Hubbard model [20, 21], temperature effects are taken into account in the broadening of energy levels $\delta \sim T$, which can be interpreted as the effect of the imaginary part of the mass operator. On the other hand, at a finite temperature, the possibility of thermal population of excited states of the system should not be disregarded. In our approach, such a population can be taken into account explicitly allowing for new transitions from excited levels (see Fig. 2) with the corresponding filling factors. Exploiting this possibility, we considered both of these factors simultaneously, choosing the linear temperature dependence of δ ($\delta = T$).

Figures 8 and 9 show two temperature evolutions of the density of states at $U = 0.5$ and 2, respectively. First, it can be seen that, in the entire temperature range, there is no narrow peak at the Fermi level, which is predicted by the dynamic mean field theory

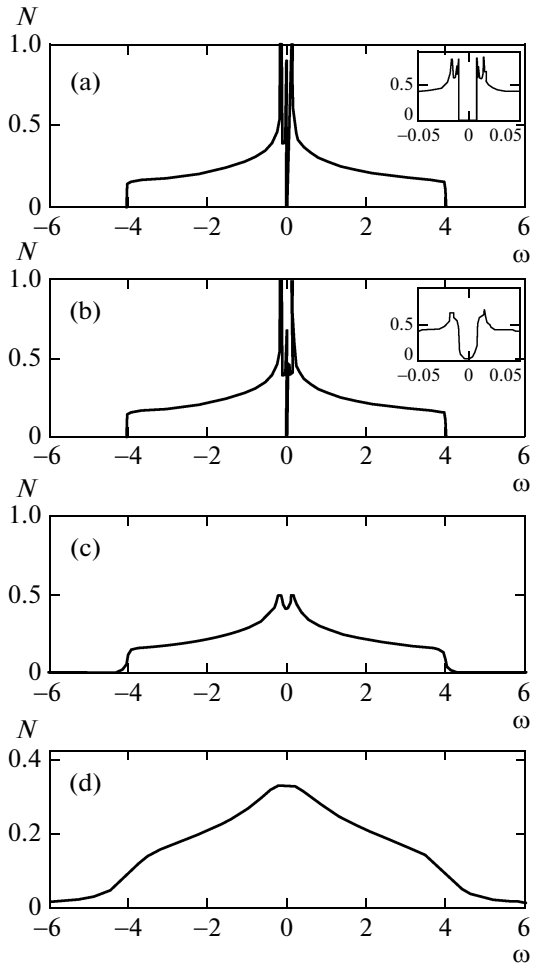

Fig. 8. Density of states for $U = 0.5$, $f = 0.997$ at temperature $T = \delta = 0.0001$ (a), 0.001 (b), 0.05 (c), and 0.5 (d).

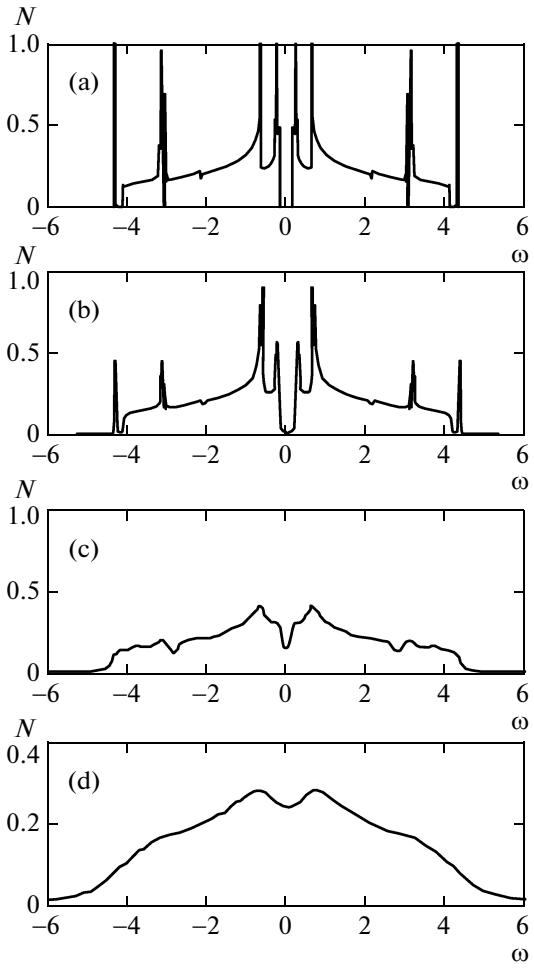

Fig. 9. Density of states for $U = 2$, $f = 0.997$ at temperature $T = \delta = 0.0001$ (a), 0.01 (b), 0.1 (c), and 0.5 (d).

(DMFT) in the vicinity of the metal–insulator transition. Conversely, at low temperatures, the gap is clearly manifested; this gap is blurred upon an increase in temperature, and a broad peak appears at a certain temperature (Fig. 8). It can be seen from Fig. 9 that at low temperatures, the density of states exhibits a large number of singularities which disappear upon heating, and two bands merge into one. This means that the state of the system experiences the metal–insulator transition at a certain temperature. It should be noted that, in this case, it is more appropriate to speak of the crossover from the insulator to the metal because the healing of the gap occurring at zero temperature occurs gradually and smoothly. Our approximation does not allow us to determine whether the electron states are localized or delocalized at the Fermi level in the pseudogap. Therefore, the transition temperature is determined only roughly as the point at which a noticeable density of states appears at the Fermi level; this approach was used in [22]. Figure 7 shows the dependence of temperature T^* of this transition on Coulomb repulsion parameter U. The value of this transition temperature is much lower than the pseudogap width in the density of states, which is formed at finite temperatures. An analogous relation between the gap width and metal–insulator transition temperature was observed in [22].

A comparison of the density of states at a finite temperature with the results obtained in [23], in which the authors used the dynamic corrections to Green's function, revealed good agreement (Fig. 10). The general pattern of the variations in the gap width as a function of parameter U is exactly the same; however, in our case, the number of singularities that appear in the density of states is larger because we precisely took into account the short-range order in the band dispersion.

The cluster version of the dynamic mean field theory (CDMFT approach) to analysis of the Hubbard model was used in [21], in which densities of states are obtained for different values of parameter U (Fig. 11c).

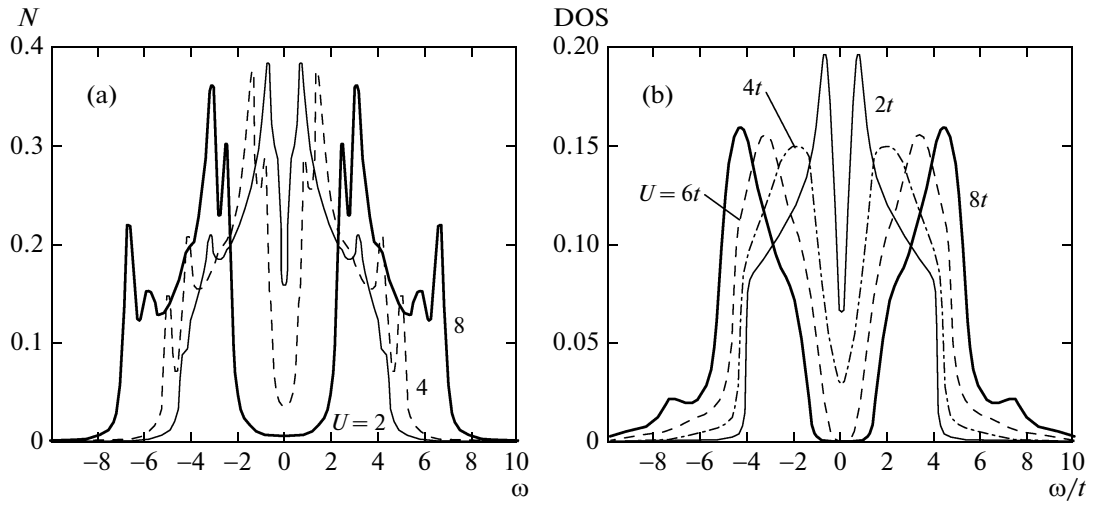

Fig. 10. Density of states at $T = 0.15$ ($\delta = 0.15, f > 0.996$): (a) our calculations; (b) borrowed from [23].

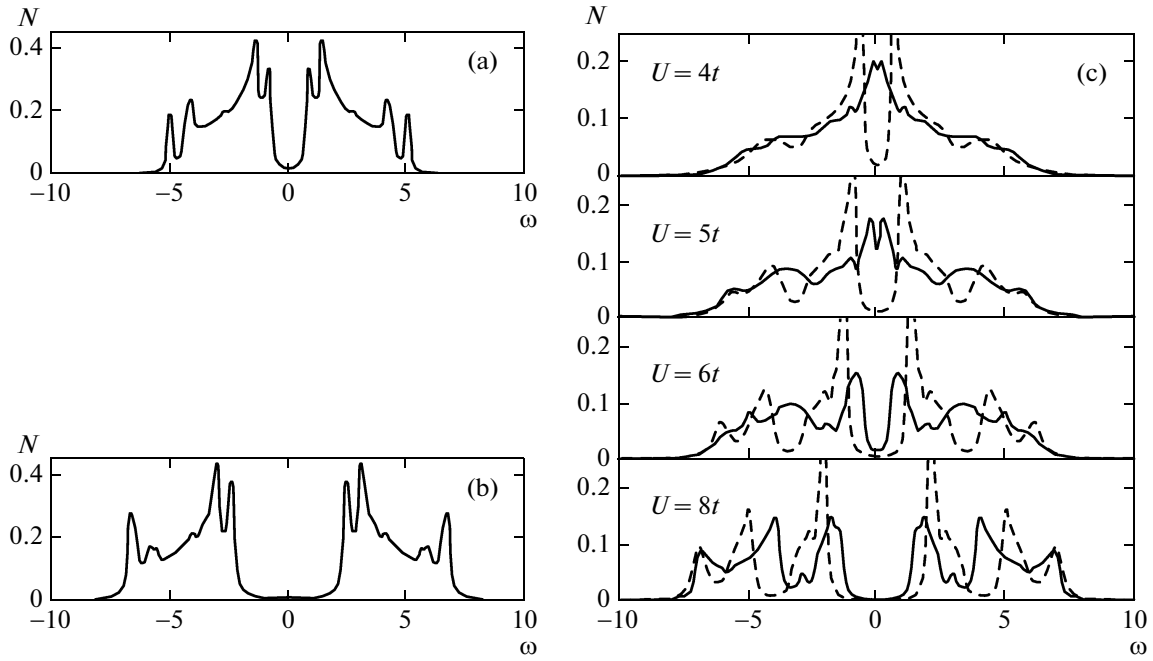

Fig. 11. Comparison of density of states for $\delta = 0.1$ for (a) $U = 4, f = 0.998$ and (b) $U = 8, f = 0.9995$ with (c) results obtained in [21]. Dashed and solid curves in (c) correspond to antiferromagnetic and paramagnetic solutions, respectively.

Calculations were performed for the paramagnetic case (solid curve in Fig. 11c), as well as the antiferromagnetic case (dashed curve in Fig. 11c). The results of our calculations (Figs. 11a and 11b) are in good agreement with the behavior of the density of states in the antiferromagnetic case. This confirms once again the conclusion that it is the short-range antiferromagnetic order that determines the band structure and the densities of states in strongly correlated systems.

7. CONCLUSIONS

The cluster perturbation theory for the 2D Hubbard model presented here demonstrates its considerable potentialities, even in the simplest case of half-filling and paves new ways for further investigations of the case with doping. Our calculations show that allowance for the short-range magnetic order plays a very important role in the formation of the band structure of strongly correlated systems. One advantage of the approach described here is the possibility to con-

trol the sum rule with the help of the f factor introduced in this approach prior to the calculation of the total Green function. The method of exact diagonalization of a cluster makes it possible to take into account the number of excited states, which ensures the fulfillment of the sum rule to a high degree of accuracy. This possibility does not exist in the case of Lanczos exact diagonalization, which is a considerable disadvantage of this approach.

The calculation of the spectral function has made it possible to obtain the spectral weights of states and revealed the shadow zone, which is not manifested in standard methods for calculating the band structure. An equally important result of this study is the observation of a gap in the density of state, which exists for indefinitely small values of Coulomb repulsion parameter U. The calculation of spin correlations functions and comparison of the density of states with the results obtained by other authors revealed that the gap opens due to the existence of the short-range antiferromagnetic order.

An analysis of the temperature dependence of the density of states shows that the peak in the density of states at the Fermi level, which is predicted by calculations based on the dynamic mean field theory, does not exist. Our calculations show that the metal–insulator transition occurs continuously upon a change in temperature. We have proved the existence of two characteristic energy scales at finite temperatures, the larger scaled being associated with the formation of a pseudogap in the vicinity of the Fermi level, while the smaller scale is associated with the metal–insulator transition temperature. We hope that the cluster perturbation theory presented here with allowance for the interaction with a large number of nearest neighbors in the case of nonzero doping level will help to reveal fundamental features of systems with strong electron correlations.

ACKNOWLEDGMENTS

The authors thank V.V. Val'kov for fruitful discussions of this work. This research was supported financially by the Russian Foundation for Basic Research (project nos. 09-02-90723-mob_st and 09-02-00127) and by program no. 5.7 of the Presidium of the Russian Academy of Sciences and integration project no. 40 of the Siberian Branch and Ural Division of the Russian Academy of Sciences.

REFERENCES

1. J. Hubbard, Proc. R. Soc. London, Ser. A **276**, 238 (1963).
2. W. Metzner and D. Vollhardt, Phys. Rev. Lett. **62**, 324 (1989).
3. A. Georges and G. Kotliar, Phys. Rev. B: Condens. Matter **45**, 6479 (1992).
4. A. Georges, G. Kotliar, W. Krauth, and M. J. Rozenberg, Rev. Mod. Phys. **68**, 13 (1996).
5. T. Maier, M. Jarrell, T. Pruschke, and M. H. Hettler, Rev. Mod. Phys. **77**, 1027 (2005).
6. A. F. Barabanov, L. A. Maksimov, and A. V. Mikheenkov, Fiz. Tverd. Tela (Leningrad) **30** (8), 2518 (1988) [Sov. Phys. Solid State **30** (8), 1449 (1988)].
7. A. F. Barabanov, L. A. Maksimov, and A. V. Mikheyenkov, J. Phys.: Condens. Matter **1**, 10 143 (1989).
8. S. G. Ovchinnikov and I. S. Sandalov, Physica C (Amsterdam) **161**, 607 (1989).
9. G. Kotliar, S. Y. Savrasov, G. Pallson, and G. Biroli, Phys. Rev. Lett. **87**, 186 401 (2001).
10. M. H. Hettler, A. N. Tahvildar-Zadeh, M. Jarrell, T. Pruschke, and H. R. Krishnamurthy, Phys. Rev. B: Condens. Matter **58**, R7475 (1998).
11. D. Senechal, D. Perez, and M. Pioro-Ladriere, Phys. Rev. Lett. **84**, 522 (2000).
12. V. V. Val'kov, V. A. Mitskan, and G. A. Petrakovskiĭ, Zh. Éksp. Teor. Fiz. **129** (2), 268 (2006) [JETP **102** (2), 234 (2006)].
13. C. Lanczos, J. Res. Natl. Bur. Stand. (USA) **45**, 255 (1950).
14. J. Jaklic and P. Prelovsek, Phys. Rev. B: Condens. Matter **49**, 5065 (1994).
15. D. Senechal, D. Perez, and D. Plouffe, Phys. Rev. B: Condens. Matter **66**, 075 129 (2002).
16. V. V. Val'kov and S. G. Ovchinnikov, *Quasiparticles in Strongly Correlated Systems* (Siberian Branch of the Russian Academy of Sciences, Novosibirsk, 2001), p. 277 [in Russian].
17. R. O. Zaĭtsev, Zh. Éksp. Teor. Fiz. **68** (1), 207 (1975) [Sov. Phys. JETP **41** (1), 100 (1975)].
18. R. O. Zaitsev, *Diagrammatic Methods in the Theory of Superconductivity and Ferromagnetism* (Editorial URSS, Moscow, 2004; Editorial URSS, Moscow, 2007), p. 175.
19. D. N. Zubarev, Usp. Fiz. Nauk **71**, 71 (1960) [Sov. Phys.—Usp. **3**, 320 (1960)].
20. Y. Z. Zhang and M. Imada, Phys. Rev. B: Condens. Matter **76**, 045 108 (2007).
21. B. Kyung, S. S. Kancharla, D. Senechal, A.-M. S. Tremblay, M. Civelli, and G. Kotliar, Phys. Rev. B: Condens. Matter **73**, 165 114 (2006).
22. S. Moukouri and M. Jarrell, Phys. Rev. Lett. **87**, 167 010 (2001).
23. T. D. Stanescu and P. Phillips, Phys. Rev. B: Condens. Matter **64**, 235 117 (2001).

Translated by N. Wadhwa